INTEGRATED OPTIMIZATION OF AILERONS FOR ACTIVE GUST LOAD ALLEVIATION

Manuel Pusch[1], Andreas Knoblach[1], and Thiemo Kier[1]

[1]German Aerospace Center
Institute of System Dynamics and Control
82234 Weßling, GERMANY
manuel.pusch@dlr.de

Keywords: Multidisciplinary Design Optimization, Aileron Design, Gust Load Alleviation, Flexible Aircraft

Abstract: An active gust load alleviation (GLA) system offers great potential for weight savings in aircraft design. Its effectiveness, however, strongly depends on the layout of available control surfaces, which is investigated in this paper. For the purpose of wing load reduction, the parameters of a static gain feedback controller are optimized simultaneously with aileron geometry parameters. Therefor, an efficient update routine for the nonlinear model of a large-scale flexible aircraft, including unsteady aerodynamics, is presented. Compared to a GLA system using the original aileron configuration, 9 % performance improvement is achieved. An additional study is carried out to quantify the necessary trade-off between individual load channels. Concluding, the significant influence of aileron size and position on overall GLA performance is clearly demonstrated and hence a consideration in preliminary aircraft design is strongly recommended.

1 INTRODUCTION

In order to allow for a more economic and environmentally friendly operation of aircraft, fuel savings are imperative. Besides the efficiency of engines and aerodynamics, the aircraft weight has a major impact on fuel consumption [1]. A reduction of aircraft weight can be achieved by using new materials like carbon composites, as it can be seen at the example of the Airbus A350 or the Boeing 787. Another approach is to decrease the design loads of the structure [2, 3] applying active control technologies. For example, the fuel consumption of the Lockheed L-1011 TriStar aircraft could be reduced by 3 % by means of active load alleviation [4]. Considering new aircraft configurations with improved lift-to-drag ratios, a special focus has to be put on gust load alleviation (GLA), as they are prone to have an increased sensitivity to atmospheric disturbances. In [5], an assessment of state of the art GLA applications is made, where the potential for weight reduction is also pointed out. In industry though, it is still practice to introduce load alleviation functions after the preliminary design phase [6], where only a limited adaption of the structure is possible. Hence, it is advantageous to include the load alleviation system already in aircraft pre-design [7]. Promising results can be achieved by multidisciplinary design optimization, where aircraft structure and load controller are designed simultaneously (see e.g. [8,9]). However, less priority is put on optimization of the layout of multifunctional control surfaces (CSs) and its concrete impact on load alleviation capability.

The aim of this paper is to investigate the effect of aileron layout on active GLA capability. In order to gain meaningful results, a flexible aircraft model of industrial complexity is considered

(Section 2). The nonlinear model includes unsteady aerodynamics and allows to compute cut loads for maneuvers as well as gust encounters. In avoidance of time consuming model rebuilding, an efficient update procedure for CS layout changes is proposed. In the derived optimization setup (Section 3), the focus lies on simultaneously optimizing controller and aileron geometry parameters to minimize the wing root bending moment (WRB). Additionally, constraints like actuator saturation, passenger comfort and stability requirements are introduced. The resulting improvement in load alleviation capability is discussed in Section 4, where the optimized aileron layout is compared with a reference configuration. Finally, a trade-off study is carried out to allow a globally balanced load reduction by prioritizing single load channels.

2 MODELING AND LOADS COMPUTATION

2.1 Structural and Aerodynamic Models

In order to consider both gust and maneuver loads, the integrated modeling approach from [10] is applied. The model is based on a linear finite element model with which a modal analysis is carried out. The resulting mode shapes are partitioned into rigid body modes $\mathbf{\Phi}_{gb}$ and flexible modes $\mathbf{\Phi}_{gf}$. Taking into account the assumptions from [11], this allows to replace the linear rigid body dynamics by the nonlinear equations of motion (EoM) from flight mechanics. Eventually, the overall EoM can be written as

$$\begin{bmatrix} m_b \left(\dot{\mathbf{V}}_b + \dot{\mathbf{\Omega}}_b \times \mathbf{V}_b - \mathbf{T}_{bE} \mathbf{g}_E \right) \\ \mathbf{J}_b \dot{\mathbf{\Omega}}_b + \mathbf{\Omega}_b \times (\mathbf{J}_b \mathbf{\Omega}_b) \end{bmatrix} = \mathbf{\Phi}_{gb}^{\mathrm{T}} \mathbf{P}_g^{\mathrm{ext}}(t), \tag{1a}$$

$$\mathbf{M}_{ff} \ddot{\mathbf{u}}_f + \mathbf{B}_{ff} \dot{\mathbf{u}}_f + \mathbf{K}_{ff} \mathbf{u}_f = \mathbf{\Phi}_{gf}^{\mathrm{T}} \mathbf{P}_g^{\mathrm{ext}}(t). \tag{1b}$$

In Equation (1a), the rigid body modes are described in the body frame of reference by the translational velocity $\mathbf{V}_b$ and the angular velocity $\mathbf{\Omega}_b$. Additionally, gravitational acceleration $\mathbf{g}_E$ is taken into account by applying a coordinate transformation $\mathbf{T}_{bE}$ from the earth fixed to the body fixed frame. It is further assumed that $\mathbf{g}_E$ as well as the inertia tensor $\mathbf{J}_b$ and the aircraft mass m_b do not change within the considered time horizon. In Equation (1b), the flexible modes $\mathbf{u}_f$ are characterized by means of the modal mass matrix $\mathbf{M}_{ff}$, the modal damping matrix $\mathbf{B}_{ff}$ and the modal stiffness matrix $\mathbf{K}_{ff}$.

The external nodal loads $\mathbf{P}_g^{\mathrm{ext}}$ include forces induced by aerodynamics, engines or landing gears. For the purpose of GLA, aerodynamic forces are of major interest. In order to consider also unsteady aerodynamics, they are obtained by means of the doublet lattice method (DLM) [12]. Applying the DLM, the lifting surfaces are discretized by trapezoidal shaped aerodynamic boxes with a control point j located at the three quarter chord respectively (see Figure 1). The orthogonal components of the flow at these control points are collected in $\mathbf{v}_j$ and normalized by the free stream velocity U_∞, leading to the downwash

$$\mathbf{w}_j = \frac{\mathbf{v}_j}{U_\infty}. \tag{2}$$

The DLM results in the unsteady aerodynamic influence coefficient (AIC) matrix $\mathbf{Q}_{jj}(k)$, which maps the downwash to the local pressure coefficients

$$\Delta \mathbf{c}_{pj} = \mathbf{Q}_{jj}(k) \mathbf{w}_j, \tag{3}$$
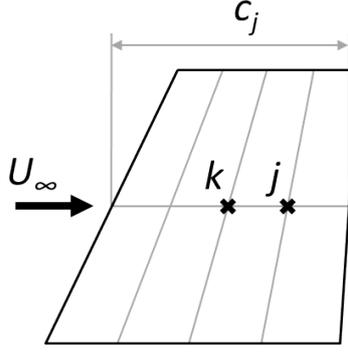
Figure 1: Aerodynamic box of chord length c_j with reference point k and control point j

where k denotes the reduced frequency parameter [12]. Note that $\boldsymbol{Q}_{jj}(k)$ is computed only at discrete frequencies and thus, it cannot be used directly for time domain simulations. To remedy this problem, a rational function approximation (RFA) is applied using Roger's method [13]. Based on the local pressure coefficients, the aerodynamic forces for each box are determined and mapped to the structural nodes by linear transformations [12]. Hence, the resulting nodal aerodynamic loads depend directly on the downwash, which can be split up into a gust-, modal- and CS-component. For the gust downwash, the continuous wind field is evaluated at each aerodynamic box and the respective orthogonal components are normalized by the free stream velocity. And the other two downwash components result from the movements of aerodynamic boxes caused by modal displacements and CS deflections. Note that the translations and rotations of aerodynamic boxes are generally described with respect to the midpoint k of each box (see also Figure 1) and hence, a transformation to the control point j is necessary. A more detailed explanation on downwash computation is given in [10] and in the next subsection, where the updating procedure for the adaption of CSs is described. Furthermore, it has to be mentioned that the aerodynamic model depends on the current Mach number, air density and free stream velocity (see also [10, 12] for details).

Eventually, the nodal loads $\boldsymbol{P}_g$ are recovered using the force summation method (FSM) [14]:

$$\boldsymbol{P}_g = \boldsymbol{P}_g^{\text{ext}} - \boldsymbol{P}_g^{\text{iner}}, \tag{4}$$

where the nodal inertial loads $\boldsymbol{P}_g^{\text{iner}}$ are obtained from the accelerations of the rigid body and flexible modes. In comparison to that, the mode displacement method (MDM) [14] computes the nodal loads by

$$\boldsymbol{P}_g = \boldsymbol{K}_{gg} \boldsymbol{\Phi}_{gf} \boldsymbol{u}_f, \tag{5}$$

using the physical stiffness matrix $\boldsymbol{K}_{gg}$. Generally, the MDM exhibits an inferior convergence behavior [15] and thus, it is not applied here. However, for interpretation of the results, the MDM is useful as it allows to determine the contributions of the corresponding flexible modes to the overall loads. Finally, the integrated cut loads $\boldsymbol{P}_c$ at critical cross sections, e.g. the wing root, are computed by a linear transformation which sums up the corresponding nodal loads.

2.2 Control Surfaces

In general, the downwash $\boldsymbol{w}_j^{\text{x}}$ caused by CS deflections $\boldsymbol{u}_x$ is described by

$$\boldsymbol{w}_j^{\text{x}} = \left(\boldsymbol{D}_{jk}^1 + s \frac{c_{\text{ref}}/2}{U_\infty} \boldsymbol{D}_{jk}^2 \right) \boldsymbol{\Phi}_{kx} \boldsymbol{u}_x, \tag{6}$$

where the CS matrix $\mathbf{\Phi}_{kx}$ maps the CS deflections to the movement of aerodynamic boxes. The mapping depends on the relative position of the box to the respective CS hinge and is determined applying a small-angle approximation. Note that, in the reverse direction, $\mathbf{\Phi}_{kx}^{\mathrm{T}}$ can be used to compute the hinge moments from the distributed loads. Additionally, the differentiation matrices $\mathbf{D}_{jk}^{1}$ and $\mathbf{D}_{jk}^{2}$ are introduced in order to transform the box displacements and movements from the reference point k to a downwash at the control point j (see also [10]). Besides, the Laplace variable is denoted by s and the reference chord length of the aircraft is c_{ref}.

When changing the geometry of a CS, it is necessary to recreate the underlying aerodynamic lattice to align it with the new boundaries of the modified CS. This, in turn, requires the AIC matrix to be recomputed and approximated again by a rational function. To avoid this rather time consuming process during optimization, an alternative approach is proposed. The AIC matrix is only computed once and the aerodynamic lattice is not further modified. Instead, the present aerodynamic boxes are assigned to the current CSs in a proportional manner.

Giving an example, the size of the original CS from Figure 2a (covered by box 4 and 6) is meant to be decreased. In Figure 2b, the aerodynamic lattice is updated, leading to a new set of aerodynamic boxes and requiring the AIC to be recomputed. In comparison to that, in Figure 2c the aerodynamic lattice is not changed but the boxes are weighted individually. For box 4 this implies, that it is weighted by a factor of 0.6 as it is covered by the new CS only by 60 %. Similarly, box 6 is weighted by 100 % meaning that it is fully assigned to the CS.

| (a) Original lattice | (b) New lattice | (c) Weighted lattice |
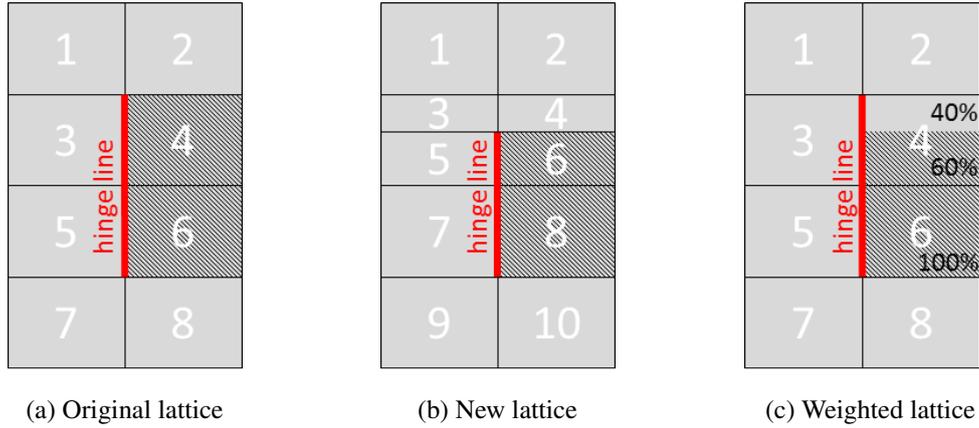
Figure 2: Example of changing the size of a CS

In summary, each box is weighted according to the percentage of its area overlapping with the respective CS. Thus, only the entries of $\mathbf{\Phi}_{kx}$ related to the modified CSs need to be updated, whereas the rest of the aircraft model remains unchanged. As the mass distribution and stiffness are assumed not to be influenced, the emerging approximation error is negligible if the size of the aerodynamic boxes is chosen sufficiently small.

2.3 Actuators and Sensors

The actuator dynamics of the CSs are modeled by a first order low pass filter

$$W_{acts}(s) = \frac{\omega_c}{s + \omega_c}, \tag{7}$$

with a bandwidth $\omega_c = 20\,\mathrm{rad/s}$. For active GLA of the wing loads, the inner and outer ailerons are primarily used, as they can be deflected in both directions allowing to affect the wing lift

distribution effectively. In addition to that, the elevators are used to compensate the pitching moment induced by aileron deflections. Furthermore, the sensor signals for feedback control are the measured pitch rate q_{meas} and the measured vertical acceleration $a_{z,meas}$ from the inertial measurement unit (IMU), which is located close to the aircraft center of gravity (CoG). These signals are readily available in common aircraft and thus, no extra sensors need to be added.

2.4 Limit Loads Computation

In order to size the structure of an aircraft, it is necessary to determine the limit loads. According to the certification requirements [2, 3], the limit loads are the lower and upper boundary of all loads occurring at any flight point including extreme flight maneuvers and severe atmospheric turbulence. Thus, the overall limit loads can be defined as

$$\boldsymbol{P}_{c,upper} = \max\left(\boldsymbol{P}_{c,upper}^{\mathrm{mvr}}, \boldsymbol{P}_{c,upper}^{\mathrm{gust}}\right) \text{ and} \tag{8a}$$

$$\boldsymbol{P}_{c,lower} = \min\left(\boldsymbol{P}_{c,lower}^{\mathrm{mvr}}, \boldsymbol{P}_{c,lower}^{\mathrm{gust}}\right), \tag{8b}$$

where the limits of both the maneuver loads $\boldsymbol{P}_c^{\mathrm{mvr}}$ and the gust loads $\boldsymbol{P}_c^{\mathrm{gust}}$ are determined as follows.

Maneuver Limit Loads

In Table 1, trim conditions for representative steady flight maneuvers, used to determine the maneuver limit loads, are listed. At each flight point, the steady horizontal flight M1G with zero pitch rate q and zero roll rate p is trimmed through the horizontal stabilizer. Additionally, the push-over maneuver MVB.nzMin and the pull-up maneuver MVB.nzMax are performed. Both maneuvers are trimmed by means of elevator deflections η and differ from each other only by the load factor n_z. The load factors $n_{z,min}$ and $n_{z,max}$ are specified in the flight maneuvering envelope (V-n diagram) [2, 3] and depend on the design airspeed. Similarly, the bidirectional rolling maneuvers MR2.nzMin and MR2.nzMax are trimmed by means of aileron deflections ξ. Moreover, sudden pilot commands are approximated by the accelerated roll maneuvers MR1_AIL.nzMin and MR1_AIL.nzMax, and the accelerated pitching maneuvers MVB_ELE.nzMin and MVB_ELE.nzMax. The extreme pilot inputs are determined by the CS deflections resulting from the previous maneuvers and are assumed to be established instantly.

name	n_z	p	$\dot{p}$	q	$\dot{q}$	η	ξ
M1G	1	0	0	0	0	0	0
MVB.nzMin	$n_{z,min}$	0	0	?	0	?	0
MVB.nzMax	$n_{z,max}$	0	0	?	0	?	0
MVB_ELE.nzMin	?	0	0	?	?	η(MVB.nzMin)	0
MVB_ELE.nzMax	?	0	0	?	?	η(MVB.nzMax)	0
MR2.nzMin	0	$\pm p_{max}$	0	?	0	?	?
MR2.nzMax	$\frac{2}{3}n_{z,max}$	$\pm p_{max}$	0	?	0	?	?
MR1_AIL.nzMin	0	0	?	?	0	?	$\pm\xi$(MR2.nzMin)
MR1_AIL.nzMax	$\frac{2}{3}n_{z,max}$	0	?	?	0	?	$\pm\xi$(MR2.nzMax)

Table 1: Trim table of maneuvers to compute limit loads

By definition, the maximum roll rate p_{max} is set to $15\,°/\mathrm{s}$ for all operation points, which is a common value for civil aircraft. Furthermore, for all maneuvers, inner and outer ailerons

are deflected equally but with opposite sign on the left and right wing. In contrast, elevators are always deflected symmetrically. Eventually, performing the described maneuvers at all considered flight points, the maneuver load boundaries $P_{c,lower}^{mvr}$ and $P_{c,upper}^{mvr}$ can be obtained.

Gust Limit Loads

In order to compute the structural loads due to atmospheric turbulence, the "1-cos" gust model according to certification requirements [2,3] is used. For wing loads, gusts in up- and downwards direction are considered as most critical. Thus, time domain simulations are carried out for only vertical gusts with different gust gradient distances varying from 9 m (30 ft) to 107 m (350 ft). Similarly as for the maneuvers, the limit loads due to gusts $P_{c,lower}^{gust}$ and $P_{c,upper}^{gust}$ result from the gust simulations performed at all considered flight points.

3 OPTIMIZATION SETUP

3.1 Controller Structure

For active GLA, a static gain feedback of the sensor signals to the actuator commands (see Section 2.3) is used. As only symmetrical gusts in vertical direction are considered (see Section 2.4), the CS deflection commands are applied equally on the left- and right-hand side. Thus, the controller outputs are $\Delta\eta_{cmd}$ for the elevators, $\Delta\xi_{inner,cmd}$ for the inner ailerons and $\Delta\xi_{outer,cmd}$ for outer ailerons. Introducing the static gain feedback matrix $\boldsymbol{K}$, the controller structure can be written as

$$\begin{bmatrix} \Delta\eta_{cmd} \\ \Delta\xi_{inner,cmd} \\ \Delta\xi_{inner,cmd} \end{bmatrix} = \boldsymbol{K} \begin{bmatrix} \Delta a_{z,meas} \\ \Delta q_{meas} \end{bmatrix}, \tag{9}$$

where all signals are referenced to the current trim conditions (denoted by the Δ). Hence, the resulting incremental actuator commands need to be added to the current actuator commands of the electronic flight control system (EFCS). For tuning, the input and output signals of the controller are normalized by their respective maximum values. The scaled elements of $\boldsymbol{K}$ are then collected in the controller tuner parameter vector $\boldsymbol{D}_K$ used for optimization (see Section 3.5).

3.2 Ailerons Parameterization

In order to evaluate the impact of the aileron layout on GLA performance, the geometry of the ailerons is parameterized. In Figure 3, different parameterizations of the span-wise position and the span of the inner and outer ailerons are given. The parameter space is limited by the minimum and maximum aileron position y_{min} and y_{max}. The former is defined by the planform break. And for the latter, the outer boundary of the reference aileron configuration, depicted in Figure 4, is taken. The ailerons should not be placed further outside as the trailing vortex at the wing tip may cause unfavorable effects [16]. For ailerons optimization, three different parameter sets $\boldsymbol{D}_{ail}$ are tested: (1) the absolute positions $y_1 \ldots y_4$, (2) the distances $\Delta y_1 \ldots \Delta y_4$, and (3) the positions y_1, y_3 combined with the aileron spans $\Delta y_2, \Delta y_4$. Furthermore, the chord of the ailerons is not changed and thus, structural integrity of the wing is maintained as the spars need not to be modified. Note that for optimization, aileron geometry constraints and parameter limits are introduced in order to avoid invalid configurations like overlaps or boundary violations.
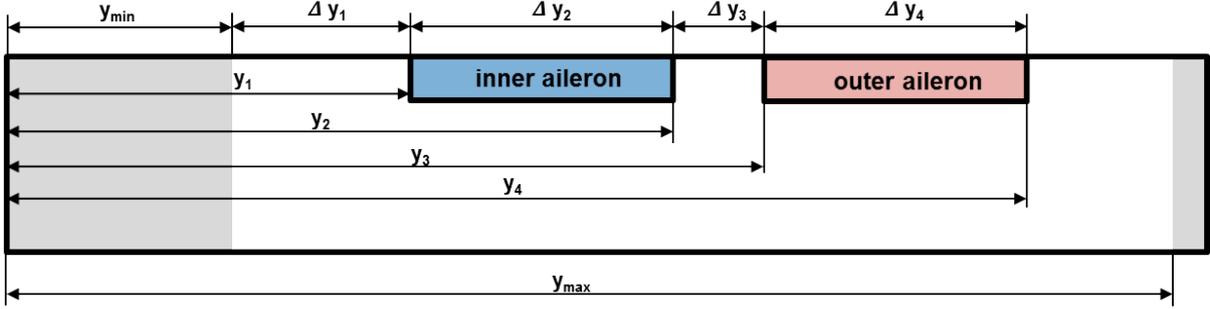
Figure 3: Ailerons parameterization
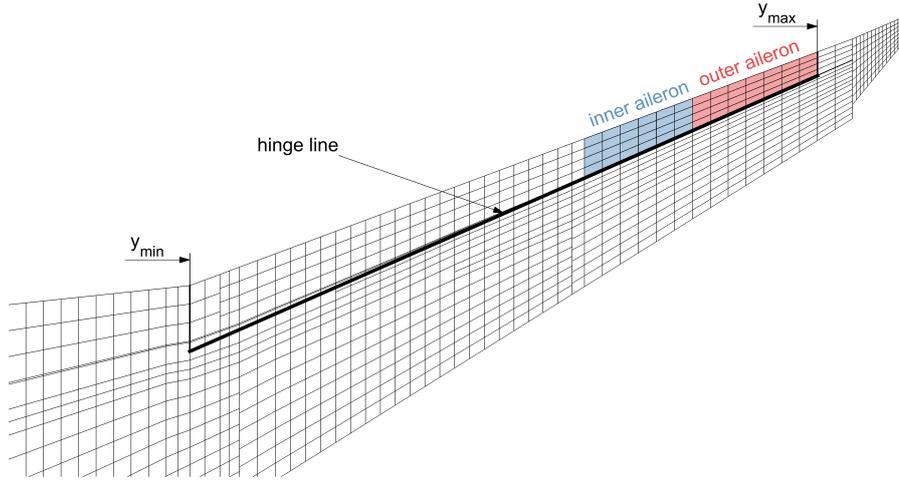
Figure 4: Reference aileron configuration with limits for layout optimization

3.3 Objective Function

The main goal for GLA controller design is to reduce the gust limit loads defined in Section 2.4. As the aircraft response to gusts can be considered as linear [10], this goal can also be captured by decreasing the gust load increments

$$\Delta \boldsymbol{P}_c^{\text{gust}} = \boldsymbol{P}_c^{\text{gust}} - \boldsymbol{P}_c^{\text{1g}}, \tag{10}$$

where $\boldsymbol{P}_c^{\text{1g}}$ are the reference loads of trimmed horizontal flight. In this paper, the focus is put on reducing the WRB since it is considered to be a major driver for the structural weight of the wing [17]. Thus, the objective function to be minimized is defined as

$$V = \max \left(\Delta P_{WRB}^{\text{gust}} \right), \tag{11}$$

which is also referred to as performance index for GLA controller evaluation.

3.4 Constraints

Limit Loads

While reducing loads at some parts of the aircraft, the GLA system might induce additional loads at other parts, e.g. at the CS mountings. Thus, it is necessary to ensure that the limit loads of

the aircraft structure (see Equation (8)) are not exceeded at any cross section. To that end, the constraint

$$C_1 : P_{c,lower} \leq P_c \leq P_{c,upper}, \tag{12}$$

is introduced, where the c-set includes all relevant cut loads for aircraft sizing.

Passenger Comfort

Furthermore, the passenger comfort should be considered during GLA controller design. Therefor, the comfort criterion f_c from [18] is applied to the vertical acceleration measurement of the IMU. The criterion is based on the ISO 2631-1 standard, which takes into account vibrating comfort and motion sickness phenomenon by weighting specific frequencies. By definition, the evaluated comfort with active GLA should not be worse than a reference comfort determined by simulations without GLA. Hence,

$$C_2 : f_c(a_{z,meas}) \leq f_c(a_{z,meas,ref}). \tag{13}$$

Note that simulations without active GLA are independent of the CS configuration, as no deflections are applied and the mass distribution is assumed not be constant (see also Section 2.2).

Stability

As static gain feedback does not guarantee any stability, a stability analysis is carried out on the linearized closed loop model of the aircraft. The resulting minimum damping ratio ζ_{min} is then compared to the reference value from the open loop case:

$$C_3 : \zeta_{min} \geq \zeta_{min,ref}. \tag{14}$$

Actuators

In order to consider actuator limitations, the allowed CS deflections are constrained by

$$C_4 : \begin{cases} \eta_{min} & \leq & \eta & \leq & \eta_{max} \\ \xi_{inner,min} & \leq & \xi_{inner} & \leq & \xi_{inner,max} \\ \xi_{outer,min} & \leq & \xi_{outer} & \leq & \xi_{outer,max} \end{cases}, \tag{15}$$

where the CS deflection boundaries are obtained from the minimum and maximum deflections of the certification maneuvers (see Section 2.4). This allows to define reasonable limitations depending on the current CS configuration and limits the CS hinge moments [19]. Furthermore, the CS deflection rates are limited by

$$C_5 : \begin{cases} \dot{\eta}_{min} & \leq & \dot{\eta} & \leq & \dot{\eta}_{max} \\ \dot{\xi}_{inner,min} & \leq & \dot{\xi}_{inner} & \leq & \dot{\xi}_{inner,max} \\ \dot{\xi}_{outer,min} & \leq & \dot{\xi}_{outer} & \leq & \dot{\xi}_{outer,max} \end{cases}, \tag{16}$$

with the maximum achievable deflection rate of all CSs being set to $80°$/s in both directions.

Handling Qualities

As ailerons are also used for lateral control of the aircraft, lateral maneuverability must be maintained. According to the certification requirements [2, 3] as well as the handling qualities requirements [20], roll performance is defined by the time a certain bank angle change can be accomplished. By defining an achievable roll rate of at least 15 °/s (see also Section 2.4), these requirements are generally fulfilled, not considering any changes in the acceleration behavior. However, roll acceleration basically depends on actuator dynamics and mass moment of inertia [16], which are both assumed not to be affected. Thus, no further handling quality constraints are introduced here.

Rigid Body Motions

Generally, the rigid body motions of an aircraft are controlled by the EFCS. Typically, the commands of the EFCS and the GLA system are superimposed, where the maneuverability of the aircraft always has to be ensured. Thus, a low-authority interaction of the GLA with the controlled rigid body motions is desired. Here, the influence of the EFCS is neglected for simplicity and instead, the pitch rate is constrained by

$$C_6 : q_{min} \leq q \leq q_{max}, \tag{17}$$

where the maximum and minimum pitch rate are derived from simulations without GLA.

3.5 Optimization Problem Formulation

Finally, the overall aeroservoelastic optimization problem can be formulated as

$$\min_{\boldsymbol{D}_K, \boldsymbol{D}_{ail}} V \text{ s.t. } C_1 \ldots C_6 \text{ are satisfied}, \tag{18}$$

with the objective function V from Section 3.3 and the constraints $C_1 \ldots C_6$ defined in Section 3.4. The design variables are the controller tuners $\boldsymbol{D}_K$ from Section 3.1 and the aileron parameters $\boldsymbol{D}_{ail}$ defined in Section 3.2. The optimization is performed with MOPS (see [21]) using a gradient based sequential quadratic programming algorithm. In each optimization step, the limit loads (Equation (8)) of the current aircraft configuration without GLA are computed. Subsequently, the GLA controller is derived, and the objectives and constraints are evaluated with respect to the actual limit loads.

4 RESULTS AND DISCUSSION

For the following results, one single flight point at an altitude of $h = 8297\,\text{m}$ and a Mach number of $Ma = 0.85$ is considered for a fully loaded aircraft. Furthermore, up- and downwards gusts with four different gust gradient distances (30 ft, 150 ft, 300 ft and 350 ft) are evaluated during optimization. Additional flight points and gusts can be taken into account easily, but have been neglected to ease result interpretation and to save computation time. Besides, the unsteady AIC matrix is computed at 8 frequency points, where the lifting surfaces are discretized by 3526 aerodynamic boxes. Subsequently, the RFA is performed with a number of 6 poles. Taking into account the first 40 flexible modes, this leads to a total number of 888 states for the nonlinear aircraft model. In order to obtain satisfying optimization results, it has been found sufficient to consider the shear force, bending- and torsional- moment at three cross sections of the wing

(including the wing root) and the root of the horizontal tail plane (HTP). Note that due to the symmetric excitation, the resulting loads and accelerations at the left- and right-hand side of the aircraft are identical and thus are only considered once. In summary, the optimization problem consists of 154 constraints, 4 objectives, and 10 tuners.

4.1 Comparison of Optimization Results

First of all, a GLA system is tuned for the reference aileron configuration depicted in Figure 5a. To that end, the optimization problem defined in Equation (18) is solved for a fixed set of aileron parameters $\boldsymbol{D}_{ail}$. The resulting reference controller reduces the peaks of the WRB (see Equation (11)) by 21 %. Secondly, geometry parameters of inner and outer ailerons are optimized simultaneously with controller tuners. As a result, the maximum WRB can be reduced in total by 30 %, which means that the GLA performance can be improved by 9 % using the optimized aileron geometry depicted in Figure 5b. For both GLA systems, the critical gust gradient distance is 300 ft, which also coincides well with Pratt's critical gust gradient distance of 12.5 reference chord lengths [22]. The respective time signals of the loads at the wing root and the true CS deflections for load alleviation are compared in Figure 6 for this critical gust, which is illustrated in the background. Additionally, the CS deflection limits for both configurations are marked in the right subplots. As already described in Section 3.4, they are determined from certification maneuvers and thus differ from each other. Generally, the deflection constraints, as well as the deflection rate bounds, are a major limiting factor for the achievable GLA performance. However, it has to be noted that for the chosen controller structure, these limitations do not necessarily come to effect at the critical gust.

(a) Reference aileron layout   (b) Optimized aileron layout
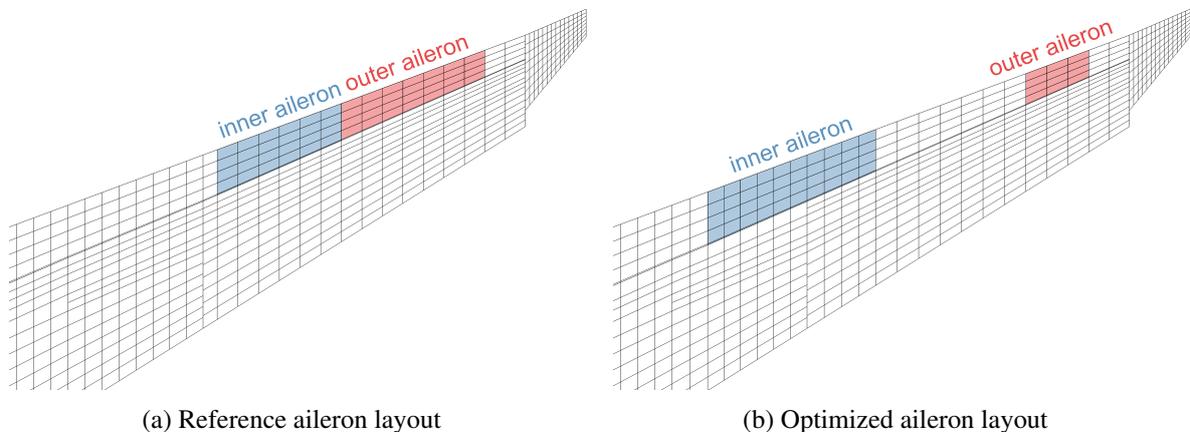
Figure 5: Comparison of aileron layouts

The reduction of the maximum WRB can be clearly seen in Figure 6a. Additionally, the shear force is reduced as well, but the torsional moment is increased. Basically, the more the WRB is reduced, the more the wing root torsional moment (WRT) is increased due to the necessary aileron deflections. This is also depicted in Figure 7, where the gust limit loads are compared over the whole wing. For a better comprehension, in the upper part of the two plots the reference aileron positions are shaded and in the lower part the optimized ones are shaded. Hence, the influence of the respective aileron layout on the torsional moment can be clearly recognized. In addition to that, the arising question of balancing the two different load channels is discussed in Section 4.3.

(a) Wing root loads
(b) CS deflections
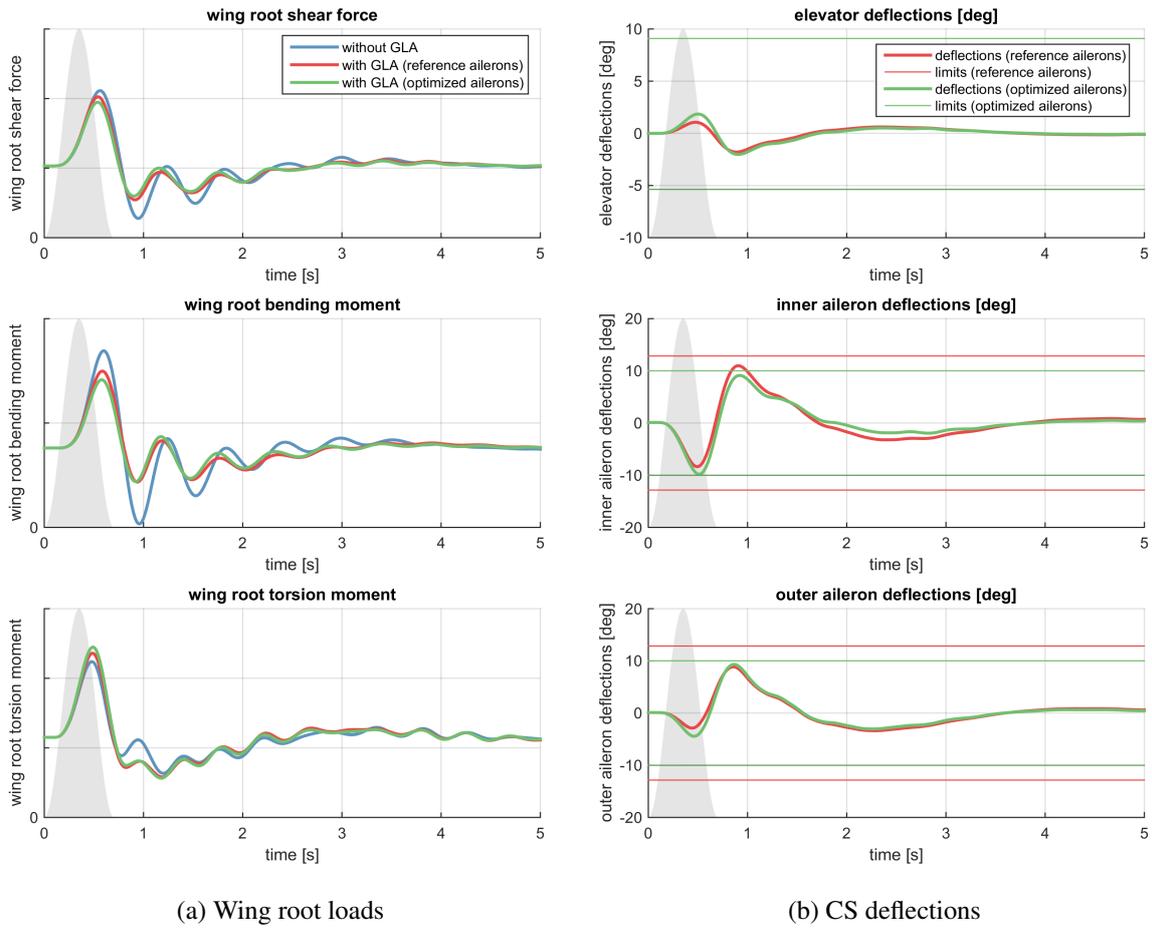
Figure 6: Comparison of time signals for critical gust
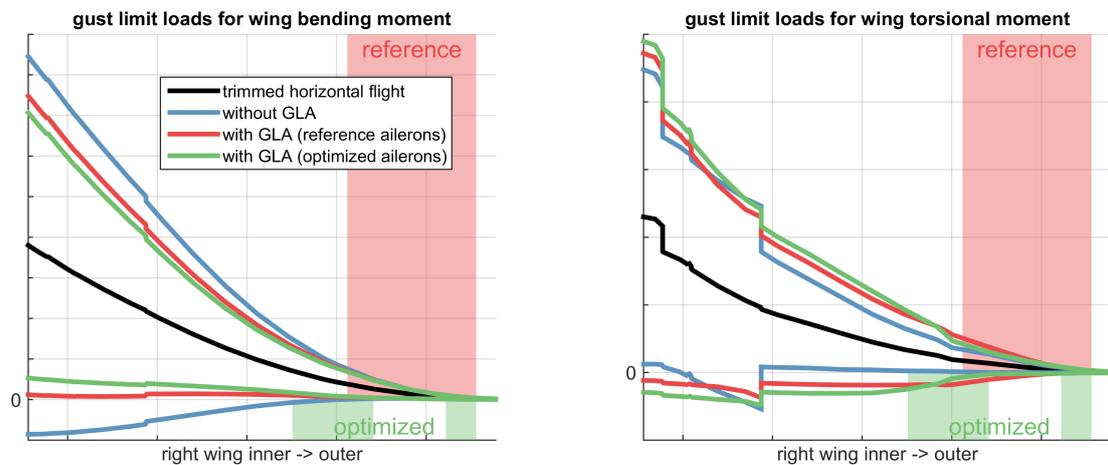
Figure 7: Comparison of bending and torsional moment on the wing

4.2 Discussion of the Optimized Aileron Layout

By varying the initial values of the tuners or the parameterization of the aileron layout, different results with similar objective values are obtained. This means, that the solution is not unique, giving additional degrees of freedom to the engineer. However, it appears that the inner ailerons are always placed similarly as depicted in Figure 5b, whereas the position and span of the outer ailerons seem to have a minor influence on GLA performance. In order to find an explanation for this result, a closer look is taken on the modal displacements leading to the maximum WRB occurring at $t \approx 0.6$ s (see Figure 6a). To that end, the contributions of each flexible mode to the WRB are computed according to the MDM (Equation (5)). The contributions are normalized by the maximum occurring WRB without GLA, and displayed in Table 2, where only the modes with the highest impact are listed. For the sake of clarity, summing up the normalized WRB contributions of *all* flexible modes would lead to the performance index V of the respective aircraft configuration. It can be seen that the WRB is clearly dominated by the first symmetric wing bending mode (#1). Hence, the GLA system should primarily damp this mode without exciting any other modes, which is assumed to be crucial when using the reference aileron layout for GLA. Comparing the first two rows of Table 2, it is shown that the contributions of the modes #10, #12 and #21 are increased applying the reference ailerons. In contrast, using the optimized ailerons for GLA, modes #10 and #12 are damped instead of excited. The reason for that might be seen in Figure 8, where the vertical wing displacements for the corresponding mode shapes are shown for the maximum WRB ($t \approx 0.6$ s). Again, in the upper part of the plot, the positions of the reference ailerons are marked, and in the lower part, the positions of the optimized ailerons are marked. The mode shapes #10 and #12 appear to be very similar for this mass case and it can be seen that the optimized inner ailerons are placed further inward than the respective oscillation node. Hence, the vertical displacements of modes #1, #10 and #12 point in the same direction at the range of the inner ailerons. For this reason, a coordinated deflection of the optimized inner ailerons may allow to damp all three mode shapes simultaneously at this instant of time. Furthermore, the undesirable excitation of mode #21 further indicates that a compromise is made for the optimal placement of the ailerons. Note that this interpretation is not unambiguous as, for instance, the solution of the optimization problem also depends on the constraints from Section 3.4.
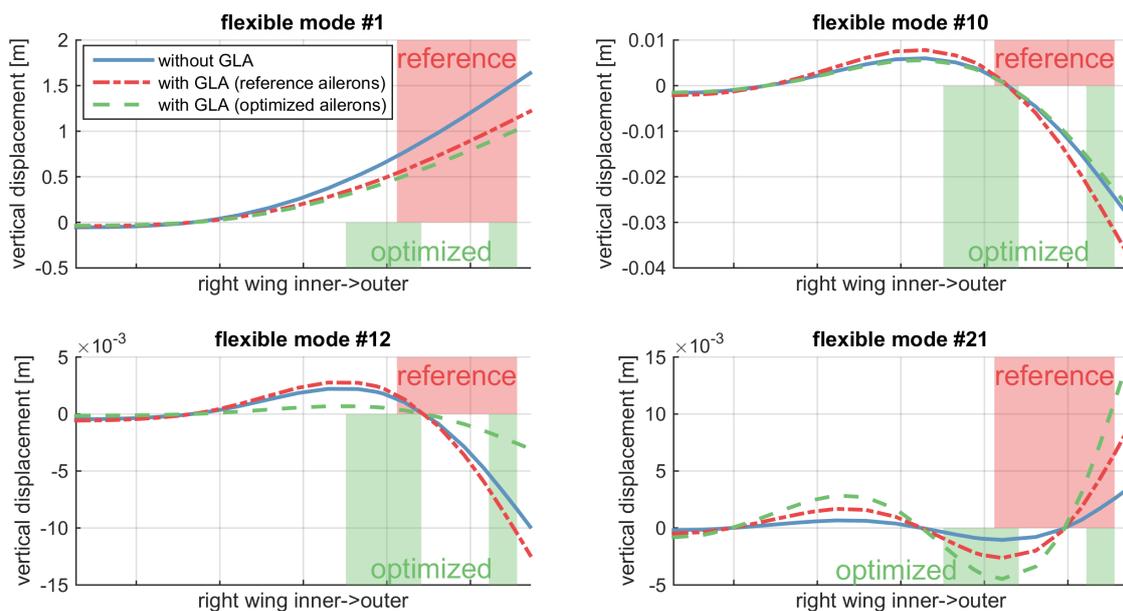
Figure 8: Comparison of modal displacements for maximal WRB

aircraft configuration	V	mode#1	mode#10	mode#12	mode#21
without GLA	100 %	93.79 %	2.72 %	1.36 %	0.82 %
with GLA (reference ailerons)	79 %	69.78 %	3.54 %	1.7 %	2.07 %
with GLA (optimized ailerons)	70 %	61.79 %	2.53 %	0.42 %	3.53 %

Table 2: Comparison of modal contributions to maximal WRB

4.3 Load Balancing

As already mentioned, actively reducing the bending moment of the wing is at the cost of the wing torsional moment. In addition to that, the loads at the HTP are increased due to the deflections of the elevators. This can also be seen in Figure 9, where the correlated gust loads of the wing root and the HTP root are compared. A trade-off study is carried out to identify the Pareto front between the WRB and the WRT. To that end, the constraints of the WRT are successively reduced and the achievable GLA performance is determined respectively. As depicted in Figure 10, it results in a monotonic decrease of the GLA performance for both the fixed reference aileron configuration and a variable aileron configuration to be optimized. If an increase of the WRT is completely suppressed, an active alleviation of the WRB is not possible, even if the aileron layout is optimized. Furthermore, not limiting the WRT at all does not lead to any better performance than already presented above. Interestingly, setting the WRT limits to the values from the reference GLA system but allowing the ailerons to be optimized, does not lead to an improvement of the GLA performance. This means that the reference aileron configuration is already optimal if no further increase of the WRT is allowed.
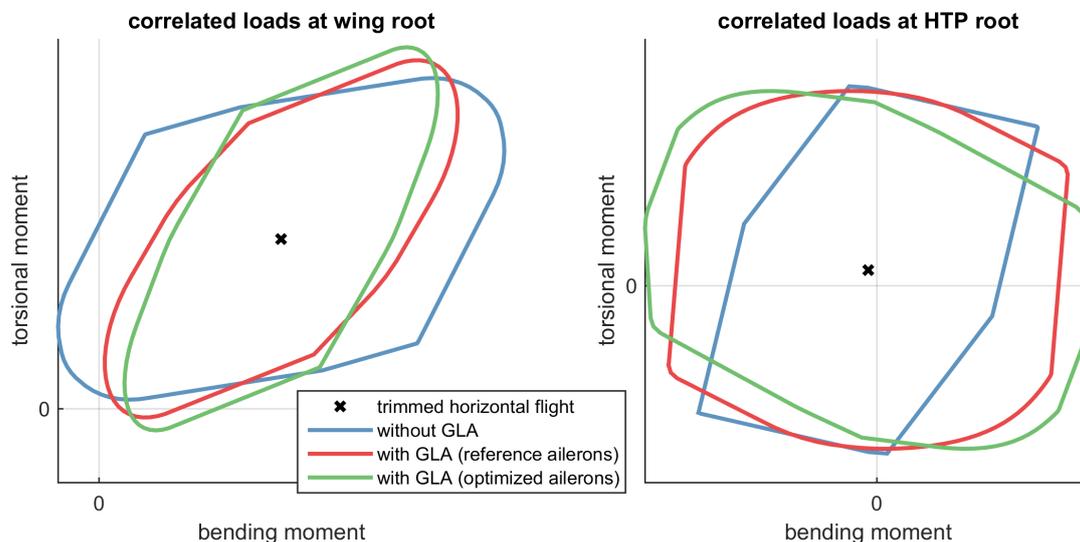
Figure 9: Comparison of correlated gust loads at wing root and HTP root

Similarly, limiting the bending moment at the root of the HTP leads to a decrease of the achievable GLA performance. Nevertheless, here, a minimum of the objective function (Section 3.3) is sought as the WRB is considered as more critical for structural sizing than the WRT or the loads at the HTP. However, any other trade-off point can also be selected taking into account further engineering aspects.
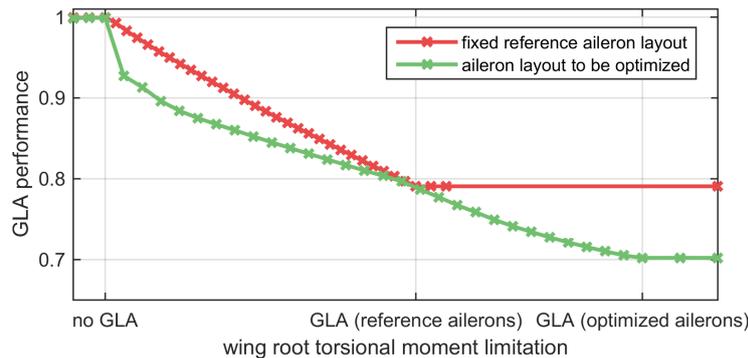
Figure 10: Comparison of achievable GLA performance depending on WRT limitation

5 CONCLUSION AND OUTLOOK

The aeroservoelastic optimization framework presented in this paper allows to simultaneously tune the controller and the CS layout for the purpose of active GLA. An efficient update routine for changes of the nonlinear aircraft model with unsteady aerodynamics is demonstrated. In order to obtain a reasonable solution, multiple constraints are introduced including limitations of loads at different cross sections, actuator bandwidth and passenger comfort. The resulting GLA system with an optimized aileron geometry allows to reduce the WRB by 30 %, whereas with the reference aileron configuration only 21 % can be achieved. An active reduction of the WRB leads to an increase of the WRT and the HTP loads, and thus, a trade-off has to be made. On the basis of single mode shapes, the optimal placement of the ailerons can be comprehended, but depends on the considered mass case. However, for future investigations, it is necessary to take into account the whole design envelope, which increases the complexity of the optimization problem. In addition to that, the interaction of the GLA system with the EFCS also has to be considered. Apart from that, further performance improvements are expected if a more advanced controller structure or additional CSs like spoilers are used. Last but not least, the concrete weight savings need to be determined in order to evaluate the impact on the direct operating costs of the aircraft.

REFERENCES

[1] International Energy Agency. *Transport, Energy and CO₂*, 2009.

[2] Federal Aviation Administration. *Federal Aviation Regulations Part 25, Airworthiness Standards: Transport Category*, 2015.

[3] European Aviation Safety Agency. *Certification Specifications and Acceptable Means of Compliance for Large Aeroplanes, CS-25, Amendment 16*, 2015.

[4] J.F. Johnston. Accelerated development and flight evaluation of active controls concepts for subsonic transport aircraft. Volume 1: Load alleviation/extended span development and flight tests. *NASA*, 1979.

[5] Christopher D. Regan and Christine V. Jutte. Survey of applications of active control technology for gust alleviation and new challenges for lighter-weight aircraft. *NASA*, 2012.

[6] A. Flaig. Airbus A380: Solutions to the aerodynamic challenges of designing the worlds largest passenger aircraft. *Royal Aeronautical Society Hamburg Branch Lecture Series*, 2008.

[7] Eli Livne. Integrated aeroservoelastic optimization: Status and direction. *Journal of Aircraft*, 36(1):122–145, Jan 1999.

[8] Sohrab Haghighat, Joaquim R. R. A. Martins, and Hugh H. T. Liu. Aeroservoelastic design optimization of a flexible wing. *Journal of Aircraft*, 49(2):432–443, 2012.

[9] Jia Xu and Ilan Kroo. Aircraft design with active load alleviation and natural laminar flow. *Journal of Aircraft*, 51(5):1532–1545, Sep 2014.

[10] Thiemo Kier and Gertjan Looye. Unifying manoeuvre and gust loads analysis models. In *International Forum on Aeroelastisity and Dynamics. Seattle, USA*, 2009.

[11] Martin R. Waszak and David K. Schmidt. Flight dynamics of aeroelastic vehicles. *Journal of Aircraft*, 25(6):563–571, 1988.

[12] W.P. Rodden and E.H. Johnson. *MSC.Nastran Version 68, Aeroelastic Analysis and User's Guide*, 2004.

[13] Kenneth L. Roger. Airplane math modelling methods for active control design. *Structures and Materials Panel*, 1977.

[14] R. Bisplinghoff, H. Ashley, and R. Halfman. Aeroelasticity, 1955.

[15] Christian Reschke. Berechnung dynamischer Lasten bei elastischen Strukturen. Master's thesis, University of Stuttgart, 2003.

[16] Mohammad H. Sadraey. *Aircraft design: A systems engineering approach*. John Wiley & Sons, 2012.

[17] Ilan Kroo. A general approach to multiple lifting surface design and analysis. *AIAA paper*, 1984.

[18] Francois Kubica and Beatrice Madelaine. Passenger comfort improvement by integrated control law design. Technical report, DTIC Document, 2000.

[19] Frederic M. Hoblit. *Gust loads on aircraft: concepts and applications*. AIAA, 1988.

[20] D. Moorhouse and R. Woodcock. *US Military Specification MIL-F-8785C*, 1980.

[21] Hans-Dieter Joos. A multiobjective optimisation-based software environment for control systems design. In *Computer Aided Control System Design, 2002. Proceedings. 2002 IEEE International Symposium on*, pages 7–14. IEEE, 2002.

[22] Kermit G. Pratt and Walter G. Walker. A revised gust-load formula and a re-evaluation of v-g data taken on civil transport airplanes from 1933 to 1950. Technical report, NACA Report No. 1206, 1954.